

Charge transfer through cross-hyperconjugated versus cross- π -conjugated bridges: an intervalence charge transfer study†

Cite this: *Chem. Sci.*, 2013, **4**, 3522

Erik Göransson,^a Rikard Emanuelsson,^b Kjell Jorner,^b Todd F. Markle,^a Leif Hammarström^{*a} and Henrik Ottosson^{*b}

Recently there has been much interest in electron transfer and transport through cross-conjugated molecules as interesting test cases for the interplay between molecular and electronic structure as well as potential motifs in the design of new compounds for molecular electronics. Herein we expand on this concept and present the synthesis and characterization of a series of four organic mixed-valence dyads to probe the effect of the bridge structure on the electronic coupling. The electronic coupling between two triarylamine units could be mediated either by cross-hyperconjugation through a saturated ER₂ bridge (E = C or Si, R = alkyl or silyl group), or *via* a cross-conjugated π -system. The aim of the study is to compare the electron transfer through the various saturated bridges to that of a cross- π -conjugated bridge. The electronic coupling in these mixed-valence compounds was determined by analysis of intervalence charge transfer bands, and was found to be in the range of 100–400 cm⁻¹. A complementary DFT and TD-DFT study indicated that the electronic coupling in the dyads with saturated ER₂ segments is highly conformer dependant. Furthermore, the calculations showed that two types of interactions contribute to the electronic coupling; a through-bond cross-(hyper)conjugation mechanism and a through-space mechanism. Taken together, these findings suggest the possibility for new architectures for molecular electronics applications utilizing cross-hyperconjugation through properly selected saturated segments which have comparable electron transfer characteristics as regular cross- π -conjugated molecules.

Received 28th March 2013

Accepted 17th June 2013

DOI: 10.1039/c3sc50844g

www.rsc.org/chemicalscience

Introduction

Recent years have witnessed substantial progress within the field of single molecule electronics.^{1,2} The majority of the molecules utilized in the field are of regular π -conjugated type, although during the last few years there has been a growing interest in molecular structures with alternative conjugation topologies such as cross- π -conjugation and σ -conjugation.^{3–10} Hyperconjugation, *i.e.*, the interaction between a local π -symmetric orbital at an unsaturated molecular segment and a local π -symmetric orbital at a saturated segment,^{11,12} is interesting both as a mediator for charge transport and as a mode of linking several π -conjugated systems.¹³ Such saturated hyperconjugated molecular segments could allow for a range of

benefits that are not achievable with purely π -conjugated molecules.

We have recently reported a study which compares cross- π -conjugation with cross-hyperconjugation of various strengths.¹⁴ Two simple π -conjugated phenylethynyl groups were covalently linked by either a single saturated moiety (CR₂ or SiR₂) or *via* a single cross- π -conjugated unit (C(=CMe₂)). The study indicated that changing the substituents, R, on the saturated center markedly affects the strength of the cross-hyperconjugation, and for that with R = SiMe₃ the cross-hyperconjugation was of similar magnitude as cross- π -conjugation on the basis of UV absorption spectroscopy, electrochemistry and density functional theory (DFT) computations.

In the present work we investigate if strong cross-hyperconjugation also translates into a similar mediation of charge transfer and charge transport as that across a cross- π -conjugated segment. *I.e.*, the study reported herein focuses on the impact of cross-hyperconjugation on a chemical process, while our earlier study primarily concerned the static electronic structures of molecules which are cross-hyperconjugated to various extents in comparison with a strongly cross- π -conjugated one.¹⁴ With this aim we designed and prepared a series of four symmetric bis-triarylamine dyads, which are bridged with units that either allow for cross- π -conjugation (D-C(=CMe₂)-D)

^aDepartment of Chemistry, Ångström Laboratory, Uppsala University, Box 523, 751 20 Uppsala, Sweden. E-mail: leif.hammarstrom@kemi.uu.se

^bDepartment of Chemistry, BMC, Uppsala University, Box 576, 751 23 Uppsala, Sweden. E-mail: henrik.ottosson@kemi.uu.se

† Electronic supplementary information (ESI) available: Details on the synthetic procedure, the analysis of spectroscopic data, the benchmarking procedure of the computational methods, the deconvolution of absorption spectra of the singly oxidized compounds, full data from the conformational scan, full reference for Frisch *et al.* [ref. 46], and absolute electronic energies and Cartesian coordinates. See DOI: 10.1039/c3sc50844g

or for cross-hyperconjugation to varying degrees (**D-Si(TMS)₂-D**, **D-Si(Me)₂-D** and **D-C(Me)₂-D**), see Chart 1. One-electron oxidation of these dyads will result in organic mixed-valence compounds,¹⁵ which allows us to study the intervalence charge transfer (IVCT) as a function of the bridging unit. Such intervalence charge transfer allows direct and more detailed insight into electronic coupling through these structures than has been previously possible. Triarylamines have previously been used as electron donor moieties in organic mixed valence compounds, because of their synthetic accessibility and the stability of the radical cation oxidized forms.^{15–19} In this paper we will present a set of new dyads and the spectroscopic and theoretical characterization of their mixed-valence behavior. We will also discuss how the electronic coupling in these dyads varies with different conformations that can be adopted. Our vision is that the findings reported herein could enable the identification and design of completely new compound classes to be used for charge transfer and transport.

Theoretical background

IVCT and mixed-valence compounds

Mixed-valence compounds are characterized by having an excess charge that can be localized on two or more (equal) sites within the molecule. Having the excess charge on a specific site corresponds to a diabatic state $|i\rangle$, and IVCT processes correspond to transitions between these states. Studies of symmetric mixed-valence compounds, notably di-ruthenium and di-osmium complexes, such as the Creutz–Taube ion, have provided many fundamental insights into the understanding of electron transfer processes.^{20–23} In the dyads in Chart 1 the possible sites for the excess charge are formally on either the “left” or “right” triarylamine, corresponding to diabatic states $|N^+, N\rangle$ and $|N, N^+\rangle$, which are denoted $|1\rangle$ and $|2\rangle$, respectively. The behavior of mixed-valence compounds is closely linked to the strength of the electronic coupling (V_{12}) between the two diabatic states. Robin and Day used this to categorize mixed-valence compounds into three general classes.²⁴ Class I represents the cases where the electronic coupling is very weak and no thermal or optical charge transfer can be observed. Class II

describes the cases for which there is a moderate electronic coupling that causes a mixing of the two diabatic states resulting in two new adiabatic states; $|a\rangle$ and $|b\rangle$ (Fig. 1). Whether a Class II compound is best described by the adiabatic or diabatic states depends on which aspects one wants to discuss. For optical IVCT the observed transition is between the adiabatic states $|a\rangle$ and $|b\rangle$. As seen in Fig. 1 the energy of this transition ($\bar{\nu}_{ab}$) can be used to approximate the Marcus reorganization energy (λ)²⁵ between the two diabatic states.²⁶ The magnitude of the optical IVCT band can also be used to calculate the electronic coupling, *vide infra*.

Class III of the Robin–Day classification describes the cases where the electronic coupling is so strong that the excess charge is delocalized over all sites. For these cases the diabatic description is clearly inappropriate and the system should be described by the two adiabatic states (Fig. 1). Optical transition between the adiabatic states $|a\rangle$ and $|b\rangle$ can often be observed and since the energy of this transition corresponds to $2V_{12}$ one can use the position of the absorption band as a direct measurement of the electronic coupling. The border between the different Robin–Day classes is not clearly defined and there are many interesting studies on mixed-valence compounds that are on the Class II/III border.^{27–31} However, the cross-conjugated bridges used in the dyads in this study should result in relatively weak couplings and are expected to show Class II behavior.

Generalized Mulliken–Hush theory

The electronic coupling between the diabatic states in a Class II compound can be extracted from the strength of the IVCT band using generalized Mulliken–Hush (GMH) theory.^{15,22,32–34} For the case where there are only two relevant states, the relationship can be summarized by eqn (1).

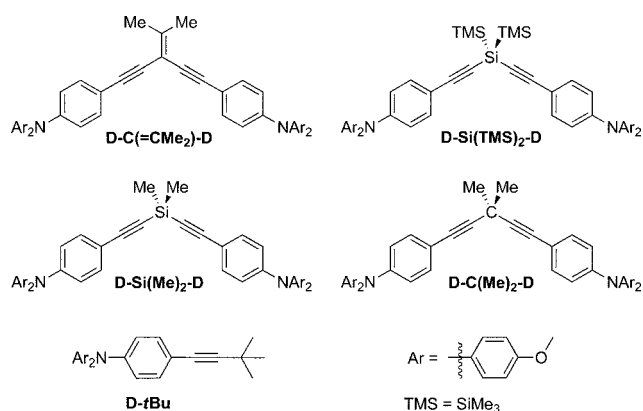


Chart 1 The investigated donor–bridge–donor systems and the 4-(*tert*-butylethynyl)-*N,N*-bis(4'-methoxyphenyl)aniline reference.

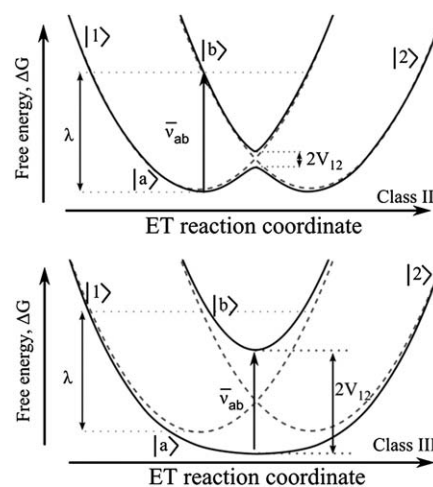


Fig. 1 Schematic description of the states in a symmetric mixed-valence compound. On top Class II and below Class III. The diabatic states, $|1\rangle$ and $|2\rangle$ are the dashed, parabolic potential energy surfaces. The adiabatic states, $|a\rangle$ and $|b\rangle$, that form through mixing of $|1\rangle$ and $|2\rangle$ are marked with solid lines. The splitting between the adiabatic states corresponds to $2V_{12}$. $\bar{\nu}_{ab}$ is the energy of the IVCT absorption band, indicated by the vertical arrow, and λ is the Marcus reorganization energy.

$$V_{12} = \frac{|\mu_{ab}| \bar{\nu}_{ab}}{|\Delta\mu_{21}|} \quad (1)$$

Here V_{12} is the electronic coupling between the diabatic states. μ_{ab} is the transition dipole moment and $\bar{\nu}_{ab}$ is the transition energy for the excitation between the two adiabatic states. $|\Delta\mu_{21}|$ corresponds to the difference in static dipole moment when an unpaired charge moves between the two adiabatic states. The transition energy ($\bar{\nu}_{ab}$) can readily be extracted from the peak position of the observed IVCT band and the transition dipole moment ($|\mu_{ab}|$) can be calculated from eqn (2a) or (2b).³⁵

$$|\mu_{ab}|^2 = \frac{3hc\epsilon_0 \ln 10}{2\pi^2 N_A} \int \frac{\epsilon(\bar{\nu})}{\bar{\nu}} d\bar{\nu} \quad (2a)$$

$$|\mu_{ab}|^2 = 3.98 \times 10^{-4} \int \frac{\epsilon(\bar{\nu})}{\bar{\nu}} d\bar{\nu} \quad (2b)$$

In eqn (2b) the constants have been evaluated and the resulting transition dipole moment will have the unit [$e\text{\AA}$], providing one expresses the extinction coefficient in [$M^{-1} \text{cm}^{-1}$].³⁶ The change in static dipole moment is most often evaluated as the movement of a point charge over a distance: $|\Delta\mu_{21}| = |r_{21}| \times e$, where $|r_{21}|$ is the charge transfer distance and e is the elementary charge. However, an exact charge transfer distance can be difficult to define, particularly with the relatively delocalized ions often found in organic systems,¹⁸ such as the radical cation of a triarylamine. For these cases it is better to evaluate $|\Delta\mu_{21}|$ from the static dipole moments of the two diabatic states, μ_1 and μ_2 .³⁷ These static dipole moments are usually most readily obtained from quantum chemical calculations, which give the values for μ_a (ground state) and μ_b (excited state) necessary to calculate μ_{21} using eqn (3).³⁴

$$|\Delta\mu_{21}| = |\mu_2 - \mu_1| = \sqrt{(\mu_b - \mu_a)^2 + 4\mu_{ab}^2} \quad (3)$$

Results and discussion

Synthesis

The donor-bridge-donor compounds were assembled in the final step from the separate donor and bridge segments (Scheme 1). The donor fragments were synthesized from a triarylamine moiety and following iodination to **1**, and subsequent Sonogashira chemistry, **2**, **3** or **D-tBu** could be achieved in accordance with the method by Lambert *et al.*³⁸ We have previously shown how the different bridge segments can be synthesized,¹⁴ and we assembled the cross- π -conjugated **D-C(=CMe₂)-D** from **4** using Sonogashira chemistry with *in situ* deprotection of the trimethylsilyl (TMS) groups. Similarly, compounds **D-Si(TMS)₂-D** and **D-C(Me)₂-D** were constructed from the iodotriarylamine **1** and bis-alkynes **5** and **6**, respectively. The SiMe₂ bridged **D-Si(Me)₂-D**, on the other hand, was assembled *via* a substitution reaction between **3** and dichlorodimethylsilane (see ESI for synthetic procedures[†]).

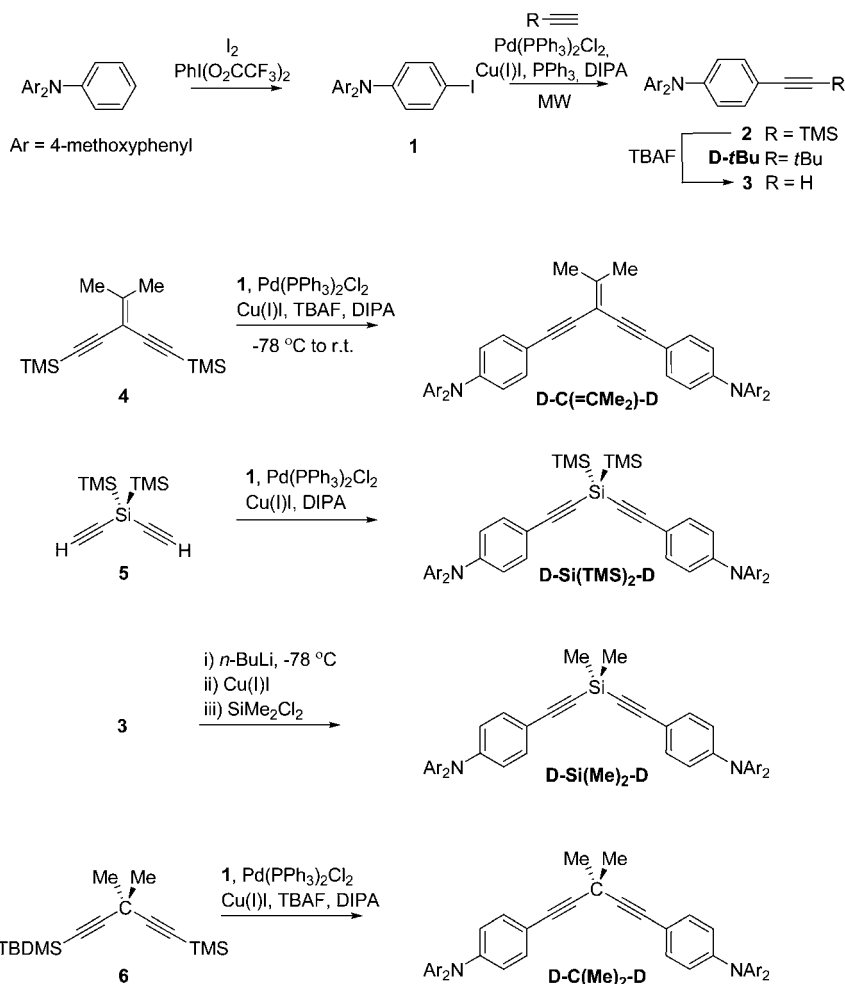
Spectroscopic and electrochemical characterization

Cyclic voltammetry on the dyads and the reference compound bearing a single triarylamine group were performed in acetonitrile (0.1 M TBAPF₆, MeCN). Although each dyad bears two triarylamines, the cyclic voltammograms display a single wave corresponding to a two-electron oxidation (ESI Fig. S8[†]). These two-electron waves are situated at similar potentials as the reference compound (**D-tBu**), but with larger peak separation between cathodic and anodic waves (ΔE_p), Table 1. These voltammograms suggest that the two triarylamine moieties are oxidized sequentially, but at potentials that are too close to be resolved by CV (this conclusion is consistent with chemical oxidation experiments described below). From the ΔE_p values we estimate that the two oxidation potentials are separated by 40–80 mV.³⁹ This small degree of electrochemical splitting is an indication that the interaction between the two triarylamines in these cross-conjugated dyads is fairly weak.

The absence of a distinct potential window where the dyads would be oxidized only once complicates the use of spectroelectrochemistry as a method to detect and characterize the singly oxidized species. Instead, titration with a chemical oxidant was used to afford the spectra of the singly oxidized species. Cu(ClO₄)₂ proved to be an efficient and convenient oxidant for these experiments (**Caution**: perchlorate salts are explosion hazards!). The moderate potential of Cu²⁺ in MeCN (*ca.* +0.55 V vs. Fc⁺⁰) is sufficiently strong to rapidly oxidize each triarylamine moiety once, but not more. The Cu²⁺ and Cu⁺ salts are relatively transparent in the region of interest,⁴⁰ and the triarylammonium radical cations are stable in the presence of Cu⁺ product. Alternatively, use of Cu(BF₄)₂ salts resulted in somewhat increased decomposition of the radical product, and NOBF₄ oxidations were slow under these conditions. Addition of Cu(ClO₄)₂ to MeCN solutions of the colorless triarylamines yielded deep blue solutions, characteristic of the radical cation product. Fig. 2 and Table 1 show the results from the titration experiments. The procedure for extracting the spectra of the neutral, singly oxidized and doubly oxidized forms of the dyads is detailed in the ESI (ESI Fig. S6[†]).

The electronic spectra of the Si(TMS)₂, Si(Me)₂ and C(Me)₂ bridged dyads are very similar in all three forms, with only small shifts of the peak positions (Fig. 2). However, for **D⁺-C(Me)₂-D** there is an additional broad peak around 8500 cm⁻¹. The cross- π -conjugated dyad, **D-C(=CMe₂)-D**, differs from the other dyads by having broader radical cation absorption peaks in both of its oxidized forms. This could be due to increased length of the conjugated system, or increased interaction between the two triarylamine moieties. The spectra of the singly and doubly oxidized species are dominated by the intense and relatively sharp band at $\sim 13\,500 \text{ cm}^{-1}$ from the triarylamine radical cation, and the spectra of the doubly oxidized dyads are similar in shape to those of the singly oxidized species, but with twice the molar absorptivity. This is another indication of weak (Class II) electronic coupling between the triarylamine moieties in these dyads.

However, close examination of the spectral region between 5000 and 15 000 cm⁻¹ reveals that there are differences



Scheme 1 Synthesis of the four dyads and the reference compound.

between the singly and doubly oxidized forms of the dyads (Fig. 3). The singly oxidized mixed-valence complexes have an additional absorption feature in the near-IR ascribed to an IVCT band. The band is most clearly seen for **D-C(Me)₂-D**, where the singly oxidized species has a distinct peak at *ca.* 8000 cm⁻¹. For the other three dyads the IVCT band appears as a shoulder on the low energy side of the radical band. In

order to get a reliable fit of the IVCT shoulder the whole spectrum was deconvoluted by fitting it with a series of Gaussian peaks. Gaussian deconvolution of the band ascribed to the IVCT band is shown in Fig. 3. The parameters for the IVCT peaks are summarized in Table 2. Details of the procedure and results of the spectral deconvolution can be found in the ESI (ESI Fig. S9–S14[†]).

Table 1 Summary of absorption and electrochemical data measured in acetonitrile

	Absorption ^a λ _{max} /nm (ε/10 ³ M ⁻¹ cm ⁻¹)			K _{disp} ^b	E _{1/2} (TPA ⁺⁰) ^c /mV vs. Fc ⁺ /Fc	ΔE _p ^d /mV
	Neutral	Singly oxidized	Doubly oxidized			
D-tBu	315 (17)	381 (22), 413 (12), 748 (35)			329	67
D-Si(TMS)₂-D	324 (49)	340 (33), 370 (30), 411 (12), 752 (34)	374, (46), 412 (24), 754 (68)	0.05	^e	^e
D-Si(Me)₂-D	330 (52)	342 (34), 376 (29), 418 (14), 753 (34)	380 (47), 420 (29), 754 (69)	0.1	348	92
D-C(Me)₂-D	325 (54)	320 (34), 379 (31), 413 (17), 749 (39), 1180 (1.4)	379 (50), 414 (31), 751 (84)	0.1	315	80
D-C(=CMe₂)-D	294 (47) 346 (76)	294 (43), 356 (48) 418 (19), 751 (35)	276 (34), 377 (42) 450 (21), 756 (67)	0.03	313	76

^a Position and extinction coefficient for observed peaks. ^b Equilibrium constant for the disproportionation reaction of singly oxidized species, determined from the titration data (relative uncertainties are ~30%). ^c Half-wave potential for the first oxidation wave. In the dyad systems, the first and second oxidation merged into a two-electron wave. ^d Peak separation between the cathodic and anodic waves. ^e Not measured.

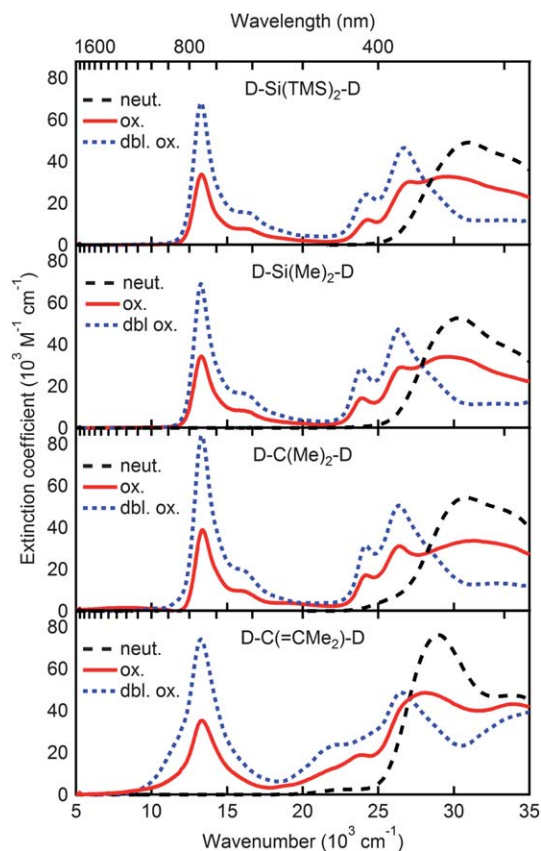


Fig. 2 Absorption spectra in MeCN for the neutral (dashed), singly (line) and doubly oxidized forms (dotted) of the four dyads. Method for extracting the extinction coefficients are described in the ESI†

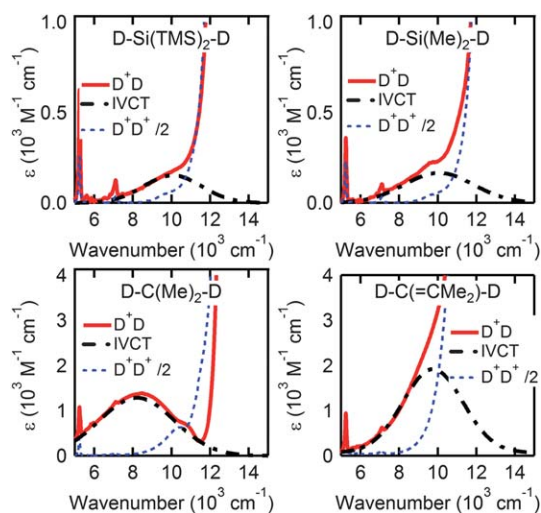


Fig. 3 Expanded view of the absorption features in the NIR region for the singly oxidized (line) and doubly oxidized (dotted) forms of the four dyads. The doubly oxidized species have been scaled down by a factor of two so that the localized radical band is at $\sim 13\,500\text{ cm}^{-1}$ has the same strength as in the singly oxidized species. The dashed-dotted lines represent the IVCT bands and come from a spectral deconvolution of the absorption spectra. (See ESI for a complete set of Gaussian peaks derived from the spectral deconvolution.†) The sharp features at ~ 5200 and $\sim 7500\text{ cm}^{-1}$ are due to incomplete background subtraction.

Computational results

Geometry optimizations of the singly oxidized forms of the four dyads, using PBE0/6-31G(d) and a polarizable continuum model for the acetonitrile solvent, resulted in geometries where the electron hole is localized to one of the two triarylamines. This agrees with the electronic spectra (Fig. 2) and our expectation that the dyads would fall into Robin–Day Class II. Preliminary geometry optimizations also resulted in a wide distribution in the geometries of the conformers adopted by the four dyads. The most notable differences were in the degree of rotation of the two inner phenylene groups relative to the ethynylene bridge unit. Since the barrier for these rotations about acetylene units can be expected to be small, we wanted to investigate to what extent the geometry and conformational freedom could affect the electronic coupling.^{6,41} We performed relaxed conformational scans on the rotation of each of the inner phenylene groups, by independently varying the two relevant dihedral angles in steps of 30° between 0° and 150° (see experimental section and ESI Fig. S15†). The results indicated that only $\text{D}^+\text{-C(=CMe}_2\text{)-D}$ has a significant energy barrier preventing rotation, stemming from the π -conjugation between the amine and the bridge unit, but even this dyad is expected to have a substantial population of all conformations at room temperature (Fig. 4 and ESI Fig. S16†).

TD-DFT was used to calculate the three lowest excitations at each of the 36 geometries from the relaxed scan. The lowest excitation corresponds to the IVCT band and is characterized as a pure ($\sim 99\%$) $\beta\text{-HOMO} \rightarrow \beta\text{-LUMO}$ transition, with the $\beta\text{-HOMO}$ localized on the neutral triarylamine and $\beta\text{-LUMO}$ on the oxidized triarylamine. The second and third lowest excitations are transitions localized on the oxidized triarylamine and they are similar to those calculated for a single oxidized triarylamine. The calculated energies for the IVCT transitions are on the order of $4000\text{--}4500\text{ cm}^{-1}$ (Table 3), which is about a factor of two lower than the experimental values. The failure to accurately reproduce the correct transition energies for charge transfer transitions is a well-known weakness of TD-DFT,⁴² and for our systems it became evident in a benchmarking study in which the CAM-B3LYP, LC- ω PBE and PBE0 functionals were compared against experimental values (see ESI†). Yet, the main purpose of the TD-DFT calculations, and this work in general, was to study differences in electronic coupling within a series of Class II mixed-valence compounds. This makes the oscillator strength a more interesting parameter than the transition energy since it relates to the probability of a transition between the initial and final states ($|1\rangle$ and $|2\rangle$). Comparing the oscillator strengths of the four dyads we note that they all display a strong dependence on the rotational conformation (Fig. 4 and ESI Fig. S17†). For example, in all four dyads the oscillator strength is zero when the pair of dihedral angles is at either $[0^\circ, 90^\circ]$ or at $[90^\circ, 0^\circ]$, *i.e.*, when the donor and acceptor π -systems are orthogonal. However, there are also notable differences in the conformational dependence of IVCT within the series. The oscillator strength for $\text{D}^+\text{-Si(TMS)}_2\text{-D}$ and $\text{D}^+\text{-C(=CMe}_2\text{)-D}$ reaches a maximum when the two phenylene groups are in the same plane as the plane spanned by the two ethynylene groups, $[0^\circ, 0^\circ]$. In contrast, the oscillator strength

Table 2 Summary of the experimental and computed IVCT parameters used to evaluate the electronic coupling

	$\bar{\nu}_{\max}^a/10^3 \text{ cm}^{-1}$	$\bar{\nu}_{\text{FWHM}}^a/10^3 \text{ cm}^{-1}$	$\epsilon_{\max}^a/10^3 \text{ M}^{-1} \text{ cm}^{-1}$	$r_{\text{N-N}}^b/\text{\AA}$	$\Delta\mu_{21}^c/e\text{\AA}$	$ \mu_{\text{ab}} ^d/e\text{\AA}$	V_{12}^e/cm^{-1}
D-Si(TMS)₂-D	9.94	3.37	0.15	14.4	13.1	0.15	111
D-Si(Me)₂-D	10.06	4.25	0.17	13.7	13.3	0.18	133
D-C(Me)₂-D	8.24	4.64	1.37	13.6	13.0	0.59	374
D-C(=CMe₂)-D	9.75	2.66	1.85	13.7	12.1	0.47	375

^a Parameters obtained from the Gaussian fit to the IVCT band. ^b Calculated distance between the two nitrogen atoms for the conformer which contributes most to the electronic coupling. ^c Change in static dipole moment using eqn (3) and values from TD-DFT calculations. Parameters for the static dipole moments can be found in ESI Table S7.† ^d Transition dipole moments calculated from eqn (2b). The integral was numerically evaluated using the parameters from the Gaussian fit. ^e The electronic coupling calculated from eqn (1) using the parameters in Table 2.

for **D⁺-Si(Me)₂-D** and **D⁺-C(Me)₂-D** at the [0°,0°] conformation is in both cases negligible, indicating that cross-hyperconjugation in these two compounds is very weak. Instead, the latter two species have their strongest transitions at the conformations with the phenylene groups perpendicularly oriented to the plane of the two ethynylene groups, [90°,90°]. The implications of these differences will be discussed in more detail below.

To account for the conformational freedom in these systems and to compare the TD-DFT results with experimental spectra we calculated the Boltzmann weighted oscillator strength and Boltzmann and oscillator strength weighted transition energies (Table 3). Using the weighted averages and eqn (4) allowed us to deduce transition dipole moments based on the TD-DFT calculations.³²

$$|\mu_{\text{ab}}|^2 = \frac{3he^2}{8\pi^2 m_e c} \frac{f}{\bar{\nu}_{\max}} \quad (4)$$

In eqn (4) h is Planck's constant, e is the elemental charge, m_e is the mass of an electron and c is the speed of light. The oscillator strength is denoted by f and the transition energy by $\bar{\nu}_{\max}$.

The TD-DFT calculations were also used to evaluate the change in static dipole moment ($\Delta\mu_{21}$) between the initial and final state using eqn (3) (see ESI for details†). A comparison of the values for $r_{\text{N-N}}$ and $\Delta\mu_{21}$ in Table 2 shows that the effective movement of electron density is somewhat shorter than the nitrogen–nitrogen distance. When the conformational freedom is taken into account, the overall agreement between the DFT-derived V_{12} values (which span 144–392 cm^{-1}) and those calculated using experimental IVCT bands (111–375 cm^{-1}) is quite striking. Nevertheless, there are discrepancies that will be discussed in more detail below.

Trends in electronic coupling

Using GMH theory (eqn (1)) we evaluated the electronic coupling from the experimental results (Table 2). As expected the magnitude of the electronic coupling elements for these cross-(hyper)conjugated dyads are decreased relative to analogous linearly conjugated systems. For comparison, using 1,4-diethynyl-phenylene as the bridging unit results in a coupling element of $\sim 1000 \text{ cm}^{-1}$.^{28,43} However, the coupling is still significant indicating that these or

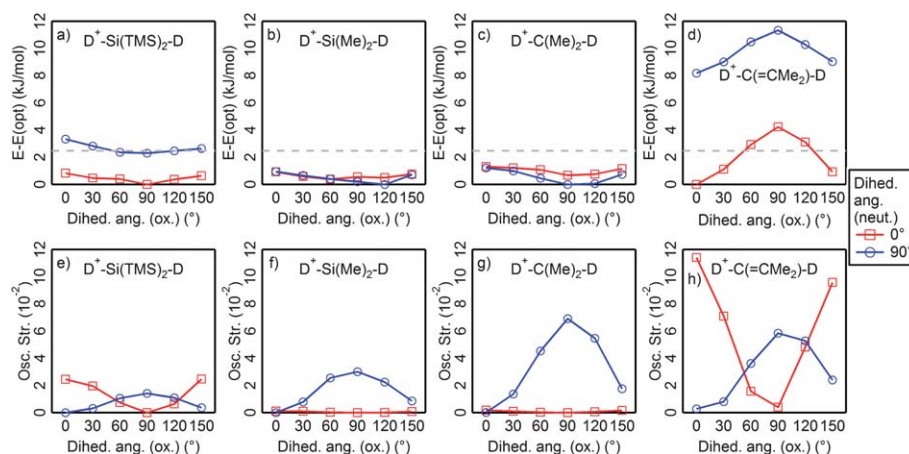


Fig. 4 Summary of the results from the conformational scan at the PBE0/6-31 G(d,p)//PBE0/6-31 G(d) level. The top four panels show the energy barrier for rotation of the inner phenylene group on the oxidized triarylamine with the inner phenylene group on the neutral side either in-plane, or perpendicular to the plane of the ethynylene bridge; *i.e.*, 0° (red squares and curve) or 90° (blue circles and curve). Changes along the x-axis correspond to rotation of the phenylethynyl group on the oxidized side. The dashed horizontal line marks the thermal energy at 298 K. The lower four panels show the conformational dependence of the oscillator strength for the IVCT transition. Note that the oscillator strength is zero for all dyads when the pair of dihedral angles is either [0°,90°] or [90°,0°]. Also note that **D⁺-Si(TMS)₂-D** and **D⁺-C(=CMe₂)-D** have the largest oscillator strength when the dihedral angles are [0°,0°], while **D⁺-C(Me)₂-D** and **D⁺-Si(Me)₂-D** have the highest transition probability at [90°,90°].

Table 3 Summary of values obtained from the TD-DFT calculations

	$E_{00}^a/10^3 \text{ cm}^{-1}$			Osc. str., (f) ^b			$\Delta\mu_{21}^c/e\text{\AA}$	$ \mu_{ab} _{\text{DFT}}^d/e\text{\AA}$	$V_{12,\text{DFT}}^e/\text{cm}^{-1}$
	$0^\circ, 0^\circ$	$90^\circ, 90^\circ$	BW	$0^\circ, 0^\circ$	$90^\circ, 90^\circ$	BW			
D-Si(TMS)₂-D	4.16	4.41	4.39	0.0246	0.0143	0.0106	13.2	0.42	156
D-Si(Me)₂-D	4.45	4.54	4.50	0.0012	0.0301	0.0090	13.3	0.43	144
D-C(Me)₂-D	4.08	4.17	4.09	0.0019	0.0596	0.0191	13.0	0.66	206
D-C(=CMe₂)-D	3.76	4.27	3.81	0.1097	0.0532	0.0657	12.3	1.32	392
D-C(TMS)₂-D^f	3.45	4.02	3.79	0.2383	0.0189	0.0974	13.5	1.54	432
D-CH₂-D^f	4.12	4.14	4.15	0.0101	0.0368	0.0115	13.2	0.51	159

^a Calculated excitation energy for the IVCT transition for the $[0^\circ, 0^\circ]$ and $[90^\circ, 90^\circ]$ conformer. BW corresponds to a Boltzmann and oscillator strength (f) weighted average for all 36 conformers. ^b Calculated oscillator strengths for the IVCT transition for the $[0^\circ, 0^\circ]$ and the $[90^\circ, 90^\circ]$ conformer. BW corresponds to a Boltzmann weighted average for all 36 conformers. ^c Change in static dipole moment calculated from eqn (3). Parameters for static dipole moments are reported in ESI Table S2.† ^d Transition dipole moment for the IVCT excitation calculated from the Boltzmann weighted oscillator strengths. Eqn (4) has been used to link the oscillator strength (f) to $|\mu_{ab}|$. ^e Electronic coupling calculated from eqn (1) using the parameters in Table 3. ^f This dyad was only studied computationally.

similar architectures are perhaps viable for molecular electronics applications. Among the four dyads it is rather surprising that the experimentally derived coupling for the cross-hyperconjugated **D-C(Me)₂-D** approaches that of the dyad with a cross- π -conjugated bridge. Furthermore, the trend in the coupling among the three ER₂ bridged dyads (C(Me)₂ > Si(Me)₂ \approx Si(TMS)₂) was not as expected from our previous results (Si(TMS)₂ > C(Me)₂ > Si(Me)₂).¹⁴ However, when conformational freedom is taken into account the theoretical investigation (Table 3) reproduces the experimental trend. The calculations do, however, predict a marked increase in V_{12} for **D-C(=CMe₂)-D** relative to the compounds with saturated ER₂-bridges. The agreement between experimental and computed values for the electronic coupling is striking, particularly because the calculated transition energies ν_{max} are underestimated by roughly a factor two. This suggests that the calculated oscillator strengths are then overestimated, resulting in a cancellation of errors. As the precise computation of oscillator strengths is strongly basis set dependent, particularly for transitions with charge transfer character, the overestimation of the present oscillator strengths is tentatively a result of the small basis set (6-31G(d,p)) used in our calculations.

Further insights into the various mechanisms of the electronic coupling in this series of compounds can be gained by examination of the trends in oscillator strength (f) calculated at the $[0^\circ, 0^\circ]$ and $[90^\circ, 90^\circ]$ conformations (as noted above, the $[0^\circ, 90^\circ]$ and $[90^\circ, 0^\circ]$ conformations have computed oscillator strengths of zero in all cases because the donor and acceptor π -systems are orthogonal).⁴¹ In the planar $[0^\circ, 0^\circ]$ conformations one observes the trend C(=CMe₂) > Si(TMS)₂ > C(Me)₂ \approx Si(Me)₂, which is what is expected for this series of cross- π -conjugated and gradually enhanced cross-hyperconjugated dyads based on our previous study.¹⁴ The calculated spin densities give a qualitative illustration of this trend (Fig. 5). Here one can see that the stronger coupling through the C(=CMe₂) bridge is due to a relatively large presence of spin density on the “neutral” side, which indicates for a strong interaction between the two states. Similarly, **D⁺-Si(TMS)₂-D** also shows a rather large spin density in the center (on the two Si-Si σ -bonds), while spin densities for **D⁺-Si(Me)₂-D** and **D⁺-C(Me)₂-D** are much lower in the center (Si-Me and C-Me σ -bonds, respectively). These trends show that

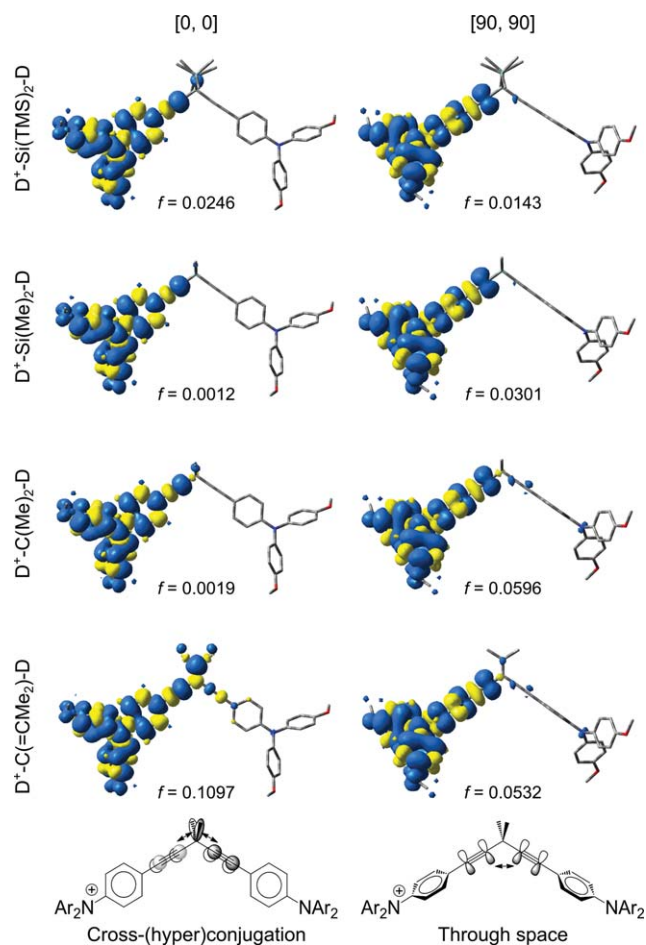


Fig. 5 Spin densities (isovalue = 0.0004) of the singly oxidized state of the four dyads (hydrogen atoms are not displayed to enhance clarity). The numbers under each conformation correspond to the calculated oscillator strengths (f). The left column shows the conformations where the inner phenylene group is in the plane spanned by the two ethynylene groups ($2 \times (\text{C}\equiv\text{C})$). This is the conformation where cross-hyperconjugation is maximal. The right column shows the conformations where the two inner phenylene groups have been rotated 90° out of the $2 \times (\text{C}\equiv\text{C})$ plane. In this conformation the coupling between the two sides occurs via direct through-space π - π interaction between the ethynylene units. The cartoons at the bottom illustrate schematically the two types of interactions.

the electronic coupling mediated through cross-hyperconjugation can be tuned *via* the R-groups.

In the $[90^\circ, 90^\circ]$ conformation, a considerably different trend for the IVCT oscillator strengths is observed; $C(\text{Me})_2 \approx C(\text{=CMe}_2) > \text{Si}(\text{Me})_2 > \text{Si}(\text{TMS})_2$. The oscillator strength and coupling for $\text{D}^+\text{-C}(\text{Me})_2\text{-D}$ is unexpectedly high, but inspection of the spin density provides an explanation. At the $[90^\circ, 90^\circ]$ conformation the close proximity of the two ethynylene groups allows for direct π - π -overlap of the in-plane orbital lobes that protrude into the space near the central atom. That the through-space π - π -overlap is generally lower in the Si-bridged dyads can be explained by the long Si-C bonds resulting in longer ethynylene-ethynylene distances. Yet, other electronic and geometric effects are also clearly contributing to the strength of the electronic coupling at this conformation.

Given the general success of our (TD-)DFT calculations in reproducing the electronic couplings determined experimentally, and in order to further probe the cross-hyperconjugation effect, we have expanded upon the series of dyads in Chart 1 computationally to include dyads bridged with $\text{ER}_2 = \text{C}(\text{TMS})_2$ and CH_2 ($\text{D-C}(\text{TMS})_2\text{-D}$ and $\text{D-CH}_2\text{-D}$). In our previous report we found that $\text{ER}_2 = \text{CR}_2$ provided increased cross-hyperconjugation when compared to $\text{ER}_2 = \text{SiR}_2$.¹⁴ Indeed, $\text{D-C}(\text{TMS})_2\text{-D}$ displays remarkable features (Fig. 6). First, DFT calculations predict that the IVCT band for $\text{D}^+\text{-C}(\text{TMS})_2\text{-D}$ would be the lowest in energy and significantly more intense than any of the other dimers in this series, more intense even than the cross- π -conjugated $\text{D-C}(\text{=CMe}_2)\text{-D}$ (Table 3). Secondly, the variation in conformational energy has a stronger resemblance with that of $\text{D-C}(\text{=CMe}_2)\text{-D}$ than for any of the ER_2 segmented dyads. Lastly, the oscillator strength at the $[0^\circ, 0^\circ]$ conformation of $\text{D-C}(\text{TMS})_2\text{-D}$ is the largest among all the dyads (more than twice that of $\text{D-C}(\text{=CMe}_2)\text{-D}$). Each of these point to a remarkably strong cross-hyperconjugative coupling, and suggest that with appropriate substituents cross-hyperconjugation can provide stronger coupling than cross- π -conjugation. The CH_2 group, on the other hand, provides for an electronic coupling which is of intermediate strength to those of $\text{C}(\text{TMS})_2$ and $\text{C}(\text{Me})_2$, indicating that the coupling strength reflects the electronegativity of the R group and the relative energy of the local $\pi(\text{ER}_2)$ orbital. The opposite trend is found for the through-space π - π interaction because for the three CR_2 segmented dyads this interaction is strongest for $\text{R} = \text{Me}$ and weakest for $\text{R} = \text{TMS}$ (see Table 3). Taken together, the TD-DFT computations reveal that these ER_2 linkers provide a structural motif that allows for tuning between weak and moderately strong couplings *via* cross-hyperconjugation, similar to what was earlier found for cross- π -conjugated bridges.⁶

In summary, there are two parallel mechanisms for mediating charge transfer in these dyads (see cartoon at bottom of Fig. 5). The first is cross- π -conjugation and cross-hyperconjugation which is most pronounced at the $[0^\circ, 0^\circ]$ conformations. The second is a through-space π - π interaction between the ethynylene units, and this is most active at the $[90^\circ, 90^\circ]$ conformation. The orbital arrangements in these two pathways for mediating charge transfer are orthogonal, and consequently, the coupling is zero at the $[0^\circ, 90^\circ]$ and $[90^\circ, 0^\circ]$ conformations.

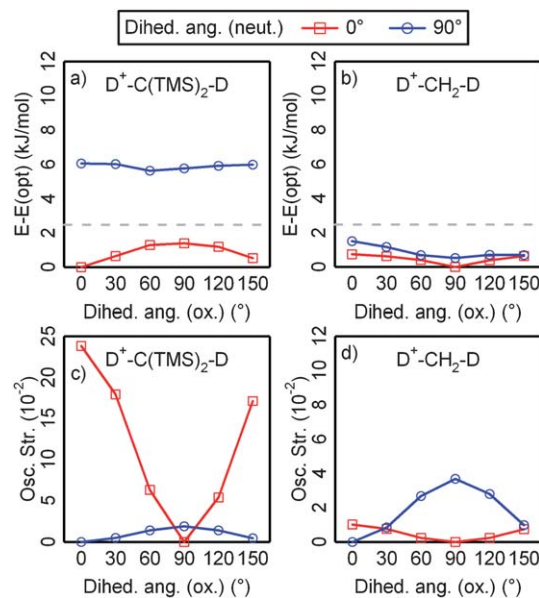


Fig. 6 Summary of the results from the conformational scans of $\text{D-C}(\text{TMS})_2\text{-D}$ and $\text{D-CH}_2\text{-D}$ at PBE0/6-31G(d,p)//PBE0/6-31G(d) level. The top two panels show the energy barrier for rotation of the inner phenylene group on the oxidized triarylamine with the inner phenylene group on the neutral side either in-plane, or perpendicular to the plane of the ethynylene bridge; *i.e.*, 0° (red squares and curve) or 90° (blue circles and curve). Changes along the x -axis correspond to rotation of the phenylethynyl group on the oxidized side. The dashed horizontal line marks the thermal energy at 298 K. The lower two panels show the conformational dependence of the oscillator strengths for the IVCT transition.

Conclusions

With this series of four dyads we have used IVCT bands to evaluate the electronic communication through cross- π -conjugated and saturated ER_2 -bridging units, which have the potential to be cross-hyperconjugated. From the analysis of the IVCT bands we may first conclude that either cross- π -conjugation or cross-hyperconjugation results in relatively weak electronic coupling. Quantum chemical calculations indicate that the electronic coupling through the bridge unit of a dyad is strongly dependent on conformation. This is another illustration of the importance of conformational freedom when one models charge transfer systems.^{6,41} The computational results also indicate that there are two viable pathways for charge transfer. The first pathway is based on the cross-(hyper)conjugation and this mechanism dominates when the inner phenylene groups are in the plane spanned by the ethynylene groups. Calculations indicate that electron releasing R-groups are required for cross-hyperconjugation in dyads with central saturated ER_2 segments, and in the case for $\text{D-C}(\text{TMS})_2\text{-D}$ computational results suggest that cross-hyperconjugation can result in stronger coupling than in the cross- π -conjugated $\text{D-C}(\text{=CMe}_2)\text{-D}$ system. The second pathway for charge mediation is *via* a through-space π - π -interaction between the two ethynylene groups. This pathway dominates when the inner phenylene groups are rotated out of the ethynylene-ethynylene plane. The strength of this mode should have a strong dependence on the distance and angle between the two ethynylene groups. Indeed, the access to two

different pathways for charge mediation should provide for design of molecules with similarly strong coupling strengths at several different conformations. Such compounds could display charge transfer and transport characteristics which are only modestly conformer dependent, a feature which could prove useful in molecular electronics applications.

Experimental section

Synthesis

All reactions were carried out using dry conditions using standard Schlenk techniques under an atmosphere of argon. Glassware was dried by the use of a heat gun at 650 °C under high vacuum. Dry solvents were obtained from a Pure Solv MD-4-EN solvent purification system. In the following, the writing "9 : 1 to 4 : 1" for eluent composition means that the eluent was changed immediately to the new proportions without intermediate steps (no gradient). Microwave-assisted chemistry was carried out in a Biotage Initiator Sixty scientific microwave reactor. The ^1H spectra were recorded at 300 or 400 MHz, and the ^{13}C spectra were recorded at 75.4 or 100.6 MHz. Referencing was made to tetramethylsilane *via* the residual solvent peaks (^1H , CDCl_3 at 7.26 ppm, C_6D_6 at 7.16 ppm; ^{13}C , CDCl_3 at 77.16 ppm, C_6D_6 at 128.0 ppm). *N,N*-Bis(4-methoxyphenyl)aniline (1), *N,N*-bis(4-methoxyphenyl)-4-[2-(trimethylsilyl)ethynyl]aniline (2) and 4-ethynyl-*N,N*-bis(4-methoxyphenyl)aniline (3) have been prepared as reported previously.³⁸ Compounds 3, 4, 5 and 6 were prepared as reported by Emanuelsson *et al.*¹⁴ Details on the synthetic procedure can be found in the ESI.†

Electrochemistry

Cyclic voltammetry was recorded with a potentiostat-galvanostat (AutoLab) controlled by the GPES 4.9 software (General Purpose Electrochemical System) using a three electrode setup. A 2 mm platinum disc electrode was employed as the working electrode, the counter electrode was a platinum wire and an AgNO_3 (10 mM, MeCN)/Ag(s) electrode was used as reference. Spectroscopic grade acetonitrile (Sigma Aldrich, Sweden), dried with 3 Å molecular sieves, was used as solvent and 0.1 M TBAPF₆ (Electrochemical grade, Sigma Aldrich) was added as supporting electrolyte. The analyte concentration was ~1 mM and after initial scans ~1 mM of ferrocene was added as an internal reference. The analyte solution was deaerated with Ar (g) for 10 min before each experiment. The potential was allowed to vary between -0.3 and +0.9 *vs.* the reference electrode with a scan rate of 0.1 V s⁻¹. All potentials are reported against Fc^+/Fc .

Spectroscopy

A Cary 5000 spectrometer was used to record absorption spectra in the visible and near IR region (300–2200 nm). The double beam setup was employed and 1 cm quartz cuvettes were used in both the reference and sample chamber. The spectra of the singly oxidized and doubly oxidized dyads was acquired *via* a series of titration experiments using copper(II) perchlorate, $\text{Cu}(\text{ClO}_4)_2$ (Sigma-Aldrich, Sweden), as a chemical oxidant. A stock solution with ~2 mM $\text{Cu}(\text{ClO}_4)_2$ in MeCN (spec. grade)

was prepared and the exact concentration of Cu^{2+} was determined from the absorption spectrum ($\epsilon_{750\text{ nm}} = 20\text{ M}^{-1}\text{ cm}^{-1}$ for $\text{Cu}(\text{ClO}_4)_2$ in MeCN). A ~1 mM stock solution was prepared for the analyte and the exact concentration was determined from titration with the oxidant. A slow degradation of the triarylamminium radicals could be observed and thus the relatively fast reaction using Cu^{2+} as oxidant (reaction complete in less than 5 s)^{44,45} was preferred compared to the slow reaction of NO^+ (5–15 min for complete reaction).²⁸ The oxygen or humidity level did not seem to accelerate the degradation of the oxidized triarylamines, but the quality of the acetonitrile was of great importance. Only spectroscopic grade acetonitrile resulted in stable aminium radicals. This may be due to reactions with amylenes, which often are added as a stabilizer to other grades of acetonitrile. The analysis of the recorded spectra was performed with Microsoft Excel and Igor Pro 6, where an example of the analytic procedure can be seen in ESI Fig. S6.†

Computational protocol

All calculations in this work have been performed with the Gaussian 09 program package⁴⁶ where the computational protocol is an adaptation to the procedure used by Renz *et al.*⁴⁷ However, instead of using their custom hybrid functional we decided to use PBE0/6-31G(d) for geometry optimization and PBE0/6-31G(d,p) for TDDFT.^{48–50} Two other functionals were also tested, LC- ω PBE^{51–54} and CAM-B3LYP,⁵⁵ but a benchmark test showed that these functionals were ill-suited for characterization of IVCT transitions. Details on the benchmarking procedure can be found in the ESI.† Each dyad was optimized in the singly oxidized form (charge: +1, multiplicity: doublet) using a solvent continuum model to stabilize the charge (IEFPCM,^{56,57} acetonitrile). At the optimized geometry we also performed TD-DFT to simulate the IVCT band. Furthermore, to probe the conformational dependence of the IVCT band potential energy surface scans on the rotation of the triarylamine moiety about the ethynylene groups were also carried out. The dihedral angle was defined as the plane spanned by the ethynylene groups and the plane created by the phenylene group bound to the ethynylene group. There are two relevant dihedral angles, one for each triarylamine, and they were scanned independent of each other in steps of 30°, between 0° and 150° (0° being when the phenylene group is in the same plane as the ethynylene groups, see ESI Fig. S15†). All other coordinates were allowed to relax at each point along the conformational scan. The conformational scan was followed by a TD-DFT calculation at each of the 16 geometries. Lastly, we also tested if expanding the basis set with diffuse function (6-31+G(d,p)) would affect the TD-DFT results, but no significant difference (see Table S1, ESI†) was found.

Acknowledgements

We are grateful for financial support from the Swedish Research Council, Knut and Alice Wallenberg foundation and Uppsala University through the U³MEC KoF07 initiative on molecular electronics. The National Supercomputer Center (NSC) in Linköping, Sweden, and the Uppsala Multidisciplinary Center for

Advanced Computational Science (UPPMAX), Uppsala, Sweden are acknowledged for generous allotment of computer time.

References

- 1 A. Aviram and M. A. Ratner, *Chem. Phys. Lett.*, 1974, **29**, 277–283.
- 2 H. Song, M. A. Reed and T. Lee, *Adv. Mater.*, 2011, **23**, 1583–1608.
- 3 G. C. Solomon, D. Q. Andrews, R. P. Van Duyne and M. A. Ratner, *J. Am. Chem. Soc.*, 2008, **130**, 7788–7789.
- 4 R. R. Tykwinski, U. Gubler, R. E. Martin, F. Diederich, C. Bosshard and P. Günter, *J. Phys. Chem. B*, 1998, **102**, 4451–4465.
- 5 R. R. Tykwinski and Y. Zhao, *Synlett*, 2002, 1939–1953.
- 6 A. B. Ricks, G. C. Solomon, M. T. Colvin, A. M. Scott, K. Chen, M. A. Ratner and M. R. Wasielewski, *J. Am. Chem. Soc.*, 2010, **132**, 15427–15434.
- 7 R. S. Klausen, J. R. Widawsky, M. L. Steigerwald, L. Venkataraman and C. Nuckolls, *J. Am. Chem. Soc.*, 2012, **134**, 4541–4544.
- 8 S. McDermott, C. B. George, G. Fagas, J. C. Greer and M. A. Ratner, *J. Phys. Chem. C*, 2009, **113**, 744–750.
- 9 D. Q. Andrews, G. C. Solomon, R. H. Goldsmith, T. Hansen, M. R. Wasielewski, R. P. V. Duyne and M. A. Ratner, *J. Phys. Chem. C*, 2008, **112**, 16991–16998.
- 10 G. C. Solomon, D. Q. Andrews, R. H. Goldsmith, T. Hansen, M. R. Wasielewski, R. P. Van Duyne and M. A. Ratner, *J. Am. Chem. Soc.*, 2008, **130**, 17301–17308.
- 11 R. S. Mulliken, *J. Chem. Phys.*, 1939, **7**, 339–352.
- 12 R. S. Mulliken, C. A. Rieke and W. G. Brown, *J. Am. Chem. Soc.*, 1941, **63**, 41–56.
- 13 I. V. Alabugin, K. M. Gilmore and P. W. Peterson, *WIREs: Comp. Mol. Sci.*, 2011, vol. 1, pp. 109–141.
- 14 R. Emanuelsson, A. Wallner, E. A. M. Ng, J. R. Smith, D. Nauroozi, S. Ott and H. Ottosson, *Angew. Chem., Int. Ed.*, 2013, **52**, 983.
- 15 A. Heckmann and C. Lambert, *Angew. Chem., Int. Ed.*, 2012, **51**, 326–392.
- 16 D. R. Kattinig, B. Mladenova, G. N. Grampp, C. Kaiser, A. Heckmann and C. Lambert, *J. Phys. Chem. C*, 2009, **113**, 2983–2995.
- 17 C. Lambert, G. Noll and J. Schelter, *Nat. Mater.*, 2002, **1**, 69–73.
- 18 S. F. Nelsen, A. E. Konradsson, M. N. Weaver and J. P. Telo, *J. Am. Chem. Soc.*, 2003, **125**, 12493–12501.
- 19 S. Amthor and C. Lambert, *J. Phys. Chem. A*, 2005, **110**, 1177–1189.
- 20 C. Creutz and H. Taube, *J. Am. Chem. Soc.*, 1969, **91**, 3988–3989.
- 21 C. Creutz and H. Taube, *J. Am. Chem. Soc.*, 1973, **95**, 1086–1094.
- 22 N. S. Hush, *Coord. Chem. Rev.*, 1985, **64**, 135–157.
- 23 D. E. Richardson and H. Taube, *Coord. Chem. Rev.*, 1984, **60**, 107–129.
- 24 M. B. Robin and P. Day, *Adv. Inorg. Chem.*, 1968, **10**, 247–422.
- 25 R. A. Marcus and N. Sutin, *Biochim. Biophys. Acta, Rev. Bioenerg.*, 1985, **811**, 265–322.
- 26 For cases where the two different adiabatic states are not isoenergetic the position of the IVCT band corresponds to the sum of the reorganization energy (λ) and the driving force (ΔG).
- 27 K. D. Demadis, C. M. Hartshorn and T. J. Meyer, *Chem. Rev.*, 2001, **101**, 2655–2686.
- 28 C. Lambert, S. Amthor and J. Schelter, *J. Phys. Chem. A*, 2004, **108**, 6474–6486.
- 29 C. Lambert and G. Nöll, *J. Am. Chem. Soc.*, 1999, **121**, 8434–8442.
- 30 B. S. Brunschwig, C. Creutz and N. Sutin, *Chem. Soc. Rev.*, 2002, **31**, 168–184.
- 31 S. D. Glover and C. P. Kubiak, *J. Am. Chem. Soc.*, 2011, **133**, 8721–8731.
- 32 C. Creutz, M. D. Newton and N. Sutin, *J. Photochem. Photobiol., A*, 1994, **82**, 47–59.
- 33 R. J. Cave and M. D. Newton, *Chem. Phys. Lett.*, 1996, **249**, 15–19.
- 34 B. S. Brunschwig, C. Creutz and N. Sutin, *Coord. Chem. Rev.*, 1998, **177**, 61–79.
- 35 W. W. Parson, *Modern Optical Spectroscopy [electronic resource]: With Examples from Biophysics and Biochemistry*, Springer-Verlag, Berlin, Heidelberg, 2007.
- 36 Debye (D) is a more common unit for dipole moments, but we chose to use [$e\text{\AA}$] as the unit, since it intuitively relates the movement of one electron over a certain distance (in \AA). $1 e\text{\AA} = 4.802 D$.
- 37 S. F. Nelsen and M. D. Newton, *J. Phys. Chem. A*, 2000, **104**, 10023–10031.
- 38 C. Lambert, G. Nöll, E. Schmälzlin, K. Meerholz and C. Bräuchle, *Chem.–Eur. J.*, 1998, **4**, 2129–2135.
- 39 A. J. Bard and L. J. Faulkner, in *Electrochemical methods: Fundamentals and applications*, Wiley, 2nd edn, 2001, ch. 12.3.6, pp. 505–509.
- 40 Cu^{2+} in acetonitrile has $\epsilon = 20 \text{ M}^{-1} \text{ cm}^{-1}$ at $\lambda_{\text{max}} = 750$. This makes this a negligible contribution to the overall absorption.
- 41 M. P. Eng and B. Albinsson, *Chem. Phys.*, 2009, **357**, 132–139.
- 42 A. Dreuw and M. Head-Gordon, *Chem. Rev.*, 2005, **105**, 4009–4037.
- 43 The coupling value of 1000 cm^{-1} is for CH_2Cl_2 as solvent and is based on a three state model of the GMH theory, which the authors prefer for systems with stronger electronic coupling.
- 44 S. Sumalekshmy and K. R. Gopidas, *Chem. Phys. Lett.*, 2005, **413**, 294–299.
- 45 K. Sreenath, C. V. Suneesh, K. R. Gopidas and R. A. Flowers, *J. Phys. Chem. A*, 2009, **113**, 6477–6483.
- 46 Frisch, M. J. and Trucks, G. W., *et al.*, Gaussian 09, Revision A.02, Wallingford CT, 2009, see ESI for complete citation.†
- 47 M. Renz, K. Theilacker, C. Lambert and M. Kaupp, *J. Am. Chem. Soc.*, 2009, **131**, 16292–16302.
- 48 C. Adamo and V. Barone, *J. Chem. Phys.*, 1999, **110**, 6158–6170.
- 49 M. M. Francl, W. J. Pietro, W. J. Hehre, J. S. Binkley, M. S. Gordon, D. J. DeFrees and J. A. Pople, *J. Chem. Phys.*, 1982, **77**, 3654–3665.

- 50 P. C. Hariharan and J. A. Pople, *Theor. Chim. Acta*, 1973, **28**, 213–222.
- 51 Y. Tawada, T. Tsuneda, S. Yanagisawa, T. Yanai and K. Hirao, *J. Chem. Phys.*, 2004, **120**, 8425–8433.
- 52 O. A. Vydrov, J. Heyd, A. V. Krukau and G. E. Scuseria, *J. Chem. Phys.*, 2006, **125**, 074106.
- 53 O. A. Vydrov and G. E. Scuseria, *J. Chem. Phys.*, 2006, **125**, 234109.
- 54 O. A. Vydrov, G. E. Scuseria and J. P. Perdew, *J. Chem. Phys.*, 2007, **126**, 154109.
- 55 T. Yanai, D. P. Tew and N. C. Handy, *Chem. Phys. Lett.*, 2004, **393**, 51–57.
- 56 J. Tomasi, B. Mennucci and R. Cammi, *Chem. Rev.*, 2005, **105**, 2999–3094.
- 57 G. Scalmani and M. J. Frisch, *J. Chem. Phys.*, 2010, **132**, 114110.